IEICE TRANS. FUNDAMENTALS, VOL.E107–A, NO.5 MAY 2024

LETTER

The Channel Modeling of Ultra-Massive MIMO Terahertz-Band Communications in the Presence of Mutual Coupling

Shouqi LI[†], ***Student Member and*** **Aihuang GUO**[†a)], ***Nonmember***

SUMMARY The very high path loss caused by molecular absorption becomes the biggest problem in Terahertz (THz) wireless communications. Recently, the multi-band ultra-massive multi-input multi-output (UM-MIMO) system has been proposed to overcome the distance problem. In UM-MIMO systems, the impact of mutual coupling among antennas on the system performance is unable to be ignored because of the dense array. In this letter, a channel model of UM-MIMO communication system is developed which considers coupling effect. The effect of mutual coupling in the subarray on the functionality of the system has been investigated through simulation studies, and reliable results have been derived.

key words: *channel modeling, UM-MIMO system, THz communication, mutual coupling*

1. Introduction

Recently, with the continuous development of society, higher wireless rates have been significantly demanded [1]. Terahertz (THz)-band communication becomes the key part of the sixth generation of communication system due to its higher bandwidth which makes Terabits-per-second (Tbps) links possible [2]. The THz-band can support a single transmission window of almost 10 THz when the distance is below one meter, while for long distance the molecular absorption effect in the transmission medium leads to a division into hundreds of transmission windows with a bandwidth of GHz [3]. Obviously, such a high bandwidth results in extremely high path loss in the free space and thus limits the communication distance. To combat that shortcoming, the ultra-massive multi-input multi-output (UM-MIMO) system with dense nano-antenna arrays has recently been proposed, which can increase the transmission rate of the communication system from both beamforming and spatial multiplexing [4]. By implementing the array-of-subarray (AoSA) structure, the entire antenna arrays can be configured for hybrid beamforming to enhance the system transmission rate [5]. Mutual coupling between antenna array elements will significantly degrade the performance of the array signal processing methods [6]. In ultra-dense antenna array structures, the effect of mutual coupling caused by the interaction of electromagnetic field among the adjacent antennas can influence the performance of system [7]. The impact of mutual coupling on nano-antenna can be quantified through coupling mode theory [8]. A frequency selective surface (FSS) decoupling structure has been designed to reduce the mutual coupling effect among adjacent antennas without changing the antenna radiation pattern [9]. In addition, the chemical potential energy has an influence on the mutual coupling effect among graphene patch antennas [10]. Regarding the channel modeling, a THz-band multiplex channel model containing line-of-sight (LoS), reflection, scattering, and diffraction can be built by ray-tracing techniques [11]. An end-to-end three-dimensional UM-MIMO system model has been proposed [12], but the impact of mutual coupling effect on system performance has not been analyzed practically.

In this letter, the incorporation of mutual coupling effect into the model of UM-MIMO communication system is focused on and the impact on system performance is analysed. The impedance-based coupling coefficient matrix is derived by building the Thevenin equivalent circuit of antenna to quantify the mutual coupling effect. With the consideration of mutual coupling, an AoSA-based end-to-end UM-MIMO channel model is developed. The impedance parameters of the graphene-based antenna are obtained through electromagnetic field simulation. The wideband channel capacity of the UM-MIMO communication system is simulated and studied, along with the impact of mutual coupling and antenna number.

The rest of this letter is organized as follows. The derivation of the coupling coefficient matrix and the design of the graphene-based antenna are presented in Sect. 2. The model of the UM-MIMO system based on the AoSA structure is created taking into account the coupling effect and is shown in Sect. 3. In Sect. 4, The influence of the number of antenna and the effect of mutual coupling on the wideband channel capacity are analysed using the model developed. Finally, conclusions are drawn in Sect. 5.

2. Mutual Coupling and Antenna Design

2.1 Coupling Matrix for Transmitter and Receiver

Mutual coupling is the phenomenon that the antenna electromagnetic field affects the phase and amplitude of others. In UM-MIMO systems, the mutual coupling becomes more obvious due to the integration of a large number of antennas in a limited area. The coupling coefficient matrix can be used to describe the mutual coupling.

Based on open circuit voltage theory, the antenna can be modelled as a Thevenin equivalent circuit. The equivalent

Manuscript received May 30, 2023.
Manuscript revised July 21, 2023.
Manuscript publicized August 23, 2023.

[†]The authors are with the Dept. of Information and Communication Engineering, Tongji University, Shanghai, 201804 China.
a) E-mail: tjgah@tongji.edu.cn

DOI: 10.1587/transfun.2023EAL2046

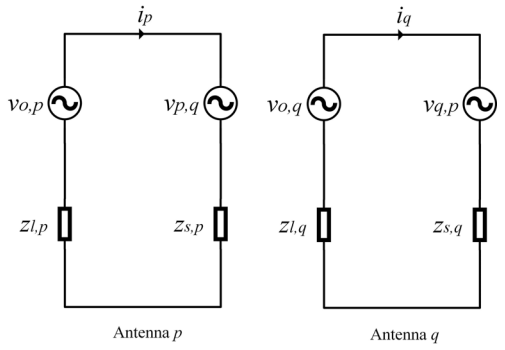

Fig. 1 Thevenin equivalent circuit of two antennas.

circuit of two antennas is shown in Fig. 1. In the equivalent circuit, $v_{o,p}$ represents the open-circuit voltage source of the pth antenna, $v_{p,q}$ denotes the coupling voltage in the pth antenna due to the mutual coupling effect between the pth antenna and qth antenna, i_p is the currency of the pth antenna, $z_{l,p}$ denotes the load-impedance of the pth antenna and $z_{s,p}$ stands for the self-impedance of the pth antenna.

Assume that there are K antennas in the transmitting array and define $v_{s,p}$ as the voltage on the self-impedance of the pth antenna. According to Kirchhoff's law, the current-voltage relationship in the transmitting array can be given by

$$\begin{cases} v_{o,1} = v_{s,1} + z_{l,1}i_1 + z_{1,2}i_2 \cdots + z_{1,K}i_K \\ v_{o,2} = v_{s,2} + z_{2,1}i_1 + z_{l,2}i_2 \cdots + z_{2,K}i_K \\ \quad \vdots \\ v_{o,K} = v_{s,K} + z_{K,1}i_1 + z_{K,2}i_2 \cdots + z_{l,K}i_K \end{cases} \tag{1}$$

which can be transformed into the vector form as

$$\boldsymbol{v}_{o,t} = \boldsymbol{v}_{s,t} + \boldsymbol{Z}_t \boldsymbol{i}_t \tag{2}$$

where $\boldsymbol{v}_{o,t} = \left[v_{o,1}, v_{o,2}, \cdots, v_{o,K}\right]^{\mathrm{T}}$ represents the open circuit voltage vector, $\boldsymbol{v}_{s,t} = \left[v_{s,1}, v_{s,2}, \cdots, v_{s,K}\right]^{\mathrm{T}}$ denotes the self-impedance voltage vector, and $\boldsymbol{Z}_t$ denotes the impedance matrix of transmitting array where the diagonal elements are load-impedances and the remaining positions are mutual-impedances. The operator $(\cdot)^{\mathrm{T}}$ represents the transpose. The current vector $\boldsymbol{i}_t = [i_1, i_2, \cdots, i_K]^{\mathrm{T}}$ can be calculated from the self-impedance vector and the voltage vector of self-impedance as $\boldsymbol{i}_t = {\boldsymbol{Z}_s}^{-1}\boldsymbol{v}_{s,t}$, where the self-impedance vector is formed as $\boldsymbol{Z}_s = \mathrm{diag}\left(z_{s,1}, z_{s,2}, \cdots, z_{s,K}\right)$. Consequently, Eq. (2) can be translated as

$$\boldsymbol{v}_{s,t} = \left(\frac{\boldsymbol{Z}_s}{\boldsymbol{Z}_s + \boldsymbol{Z}_t}\right)\boldsymbol{v}_{o,t} \tag{3}$$

Thus, the coupling coefficient matrix of the transmitting array is given by $\boldsymbol{M}_t = \boldsymbol{Z}_s\left(\boldsymbol{Z}_s + \boldsymbol{Z}_t\right)^{-1}$, which is decided by the self-impedance matrix $\boldsymbol{Z}_s$ and the transmitting array impedance matrix $\boldsymbol{Z}_t$. Based on symmetry consideration, the coupling coefficient matrix of the receiving array can be simply given by $\boldsymbol{M}_r = \boldsymbol{Z}_l\left(\boldsymbol{Z}_l + \boldsymbol{Z}_r\right)^{-1}$, which is decided by the load-impedance matrix $\boldsymbol{Z}_l$ and the receiving array impedance matrix $\boldsymbol{Z}_r$.

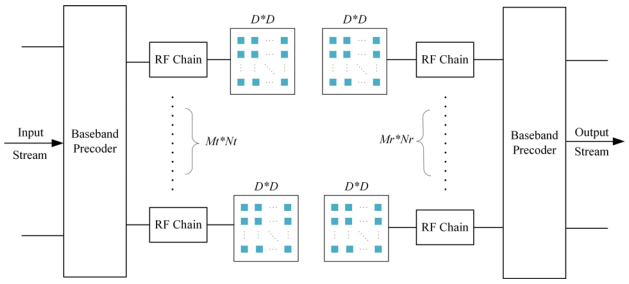

Fig. 2 Array-of-subarray (AoSA) structure.

2.2 Graphene-Based Antenna Design

To calculate the coupling coefficient matrix, the impedance parameters of the antenna are required. Therefore, a graphene-based patch antenna that can operate in the THz band is designed in this part. The graphene layer (chemical potential = 0.2 eV) of 3 nm thickness sandwiched between a silicon layer of 0.2 μm thickness ($\varepsilon_r = 11.9$, $\tan\delta = 0.00025$) and an aluminum layer of 5.5 μm thickness ($\varepsilon_r = 9.4$, $\tan\delta = 0.0004$) to form a stack structure of size $70 \times 70 \times 5.703\ \mu\mathrm{m}^3$. The stack structure is laid flat in the central silica substrate layer ($\varepsilon_r = 3.9$, $\tan\delta = 0.001$) of 3 μm in thickness while the feed line is located between the aluminum and silica layers. The graphene-based patch antenna can be simulated using simulation software to obtain the impedance characteristics required to determine the coupling coefficient matrix.

3. AoSA Architecture-Based UM-MIMO Channel Modeling

This letter considers an end-to-end UM-MIMO system based on the AoSA architecture which is shown in Fig. 2. With $M_t \times N_t$ and $M_r \times N_r$ subarrays at the transmitter and receiver ends, respectively, each consisting of $D \times D$ graphene-based antenna elements tightly grouped together. With each subarray being powered by its own radio frequency (RF) chain due to the AoSA architecture, hybrid beamforming can help overcome the high path loss in the THz band while consuming less complexity and power and relieving high-frequency hardware constraints.

Assuming that $\boldsymbol{x}$ is the $N_{in} \times 1$ transmitted signal vector, $\boldsymbol{y}$ is the $N_{in} \times 1$ received signal vector and $\boldsymbol{n}$ is the $M_r N_r \times 1$ noise signal vector, Ref. [12] points that the end-to-end UM-MIMO communication system model is represented by the function of frequency as

$$\boldsymbol{y}(f) = \boldsymbol{v}_r^{\mathrm{H}}(f)\boldsymbol{H}(f)\boldsymbol{v}_t\boldsymbol{x}(f) + \boldsymbol{v}_r^{\mathrm{H}}\boldsymbol{n}(f) \tag{4}$$

where $\boldsymbol{v}_t$ is $M_t N_t \times N_{in}$ baseband precoding vector at the transmitter, $\boldsymbol{v}_r$ is $M_r N_r \times N_{in}$ combiner vector at the receiver. $\boldsymbol{H}$ is $M_r N_r \times M_t N_t$ channel transmission matrix

among transceivers. The operator $(\cdot)^{\mathrm{H}}$ represents the conjugate transpose.

The channel transmission matrix $\boldsymbol{H}$ actually consists of the channel response $\boldsymbol{h}$ between each transmitting and receiving subarray due to the fact that the base element is subarray in the AoSA structure. The channel response between the ath subarray at the transmitter and the bth subarray at the receiver in the UM-MIMO antenna system is given by

$$\boldsymbol{h}_{a,b}(f) = \boldsymbol{s}_r^{\mathrm{H}}(\varphi_r, \theta_r) G_r \alpha_{a,b} G_t \boldsymbol{s}_t(\varphi_t, \theta_t) \tag{5}$$

where $\boldsymbol{s_r}$ and $\boldsymbol{s_t}$ are the steering vectors of the subarray at transmitter and receiver. The φ_t and φ_r represent the azimuth angles of transmitting and receiving subarray. The θ_t and θ_r represent the elevation angles of transmitting and receiving subarray. Furthermore, G_r and G_t denote the antenna gains of transceiver, and $\alpha_{a,b}$ denotes the path gain.

Because of the high path loss in the THz band, the LoS and non-line-of-sight (NLoS) reflected rays become the main components of the THz channel [13]. In the UM-MIMO system, due to the gain of hybrid beamforming used in the AoSA structure, LoS propagation becomes the only factor to be considered in the channel model. The path gain of the LoS propagation α_{LoS} is mainly determined by the molecular absorption loss and the propagation loss as

$$\begin{aligned}\alpha_{LoS} &= \frac{c}{4\pi f d} \exp \cdot (-j2\pi f \tau_{LoS}) \\ &\quad \cdot \exp\left(\frac{-\kappa(f)\, d}{2}\right)\end{aligned} \tag{6}$$

where d denotes the transmission distance, c represents the speed of light in vacuum and $\tau_{LoS} = d/c$ denotes the time-of-arrival (ToA) of LoS path. Since part of the wave energy is converted into the internal kinetic energy of the molecules of the transmission medium during transmission, the molecular absorption coefficient $\kappa(f)$ is frequency-selective. Considering the mutual coupling effect leads to a correction of the steering vectors of the transceiver subarray as

$$\begin{aligned}\boldsymbol{s}_t^{mc}(\varphi_t, \theta_t) &= \boldsymbol{M}_t \boldsymbol{s}_o(\varphi_t, \theta_t) \\ \boldsymbol{s}_r^{mc}(\varphi_r, \theta_r) &= \boldsymbol{M}_r \boldsymbol{s}_o(\varphi_r, \theta_r)\end{aligned} \tag{7}$$

where $\boldsymbol{M}_t$ and $\boldsymbol{M}_r$ denote the coupling matrices of transmitting and receiving subarray. Correspondingly, the channel transmission matrix after accommodating coupling effect can be given by

$$\boldsymbol{H}_{mc} = \begin{bmatrix} \boldsymbol{h}_{1,1}^{mc} & \cdots & \boldsymbol{h}_{1,M_t N_t}^{mc} \\ \vdots & \ddots & \vdots \\ \boldsymbol{h}_{M_r N_r, 1}^{mc} & \cdots & \boldsymbol{h}_{M_r N_r, M_t N_t}^{mc} \end{bmatrix} \tag{8}$$

Due to the unusually broad transmission window in the terahertz range, the operating band is divided into multiple sub-bands and the total channel capacity within the transmission window is obtained by calculating and summing the Shannon formula within each sub-band as

$$C = \sum_{n=1}^{N_{sub}} \triangle f \log\left(1 + \frac{|\boldsymbol{H}_{mc}(f_n)|^2 P_n}{\triangle f W}\right) \tag{9}$$

where N_{sub} is the number of sub-band, $\triangle f$ denotes the bandwidth of each sub-band. P_n represents the transmit power of the nth sub-band which is allocated using the equal power allocation algorithm. W represents the power spectral density of the additive white Gaussian noise.

4. Numerical Results

The established channel model of the UM-MIMO communication system in the presence of mutual coupling is evaluated in this section, by focusing on the impact of the number of antenna and the effect of mutual coupling on wideband channel capacity.

4.1 The Impact of Antenna Number

Based on the simulation parameters in Table 1, the UM-MIMO channel capacity is shown in Fig. 3 for the different number of subarrays and transmit power. Figure 3 shows that increasing the number of subarrays will lead to an improvement in channel capacity. In addition, the size of the subarray is another important factor. The number of subarrays is set to 8 to observe the influence of subarray size on the capacity of the UM-MIMO communication system. The Fig. 4 shows that the increase in subarray size can significantly enhance the channel capacity of the system. At the transmit power of 10 dBm, the channel capacity of the 16×16 subarray is approximately 2.62 times that of the 8×8 subarray in Fig. 4.

The above results show that increasing the number of antenna in the array brings a significant improvement in channel capacity when the size of the antenna allows. Therefore the miniaturization and densification of the antenna help to overcome the high path loss of UM-MIMO system in the

Table 1 Simulation parameters.

Parameter	Value
certer frequency	7.715THz
number of sub-band	100
sub-band bandwidth	1GHz
size of the subarray	8×8
power spectral density of AWGN	-75 dBm
antenna spacing	$\lambda/8$

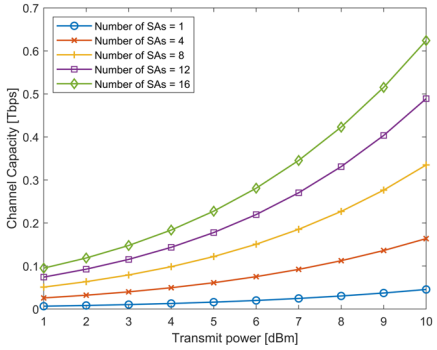

Fig. 3 UM-MIMO capacity for the different number of subarray and transmit power.

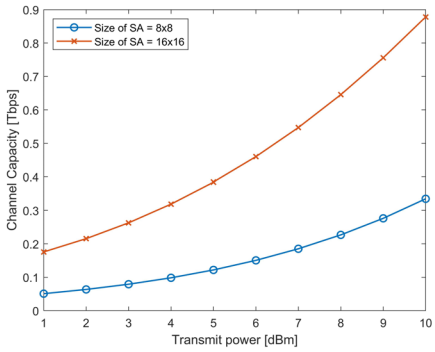

Fig. 4 UM-MIMO capacity for the different size of subarray and transmit power.

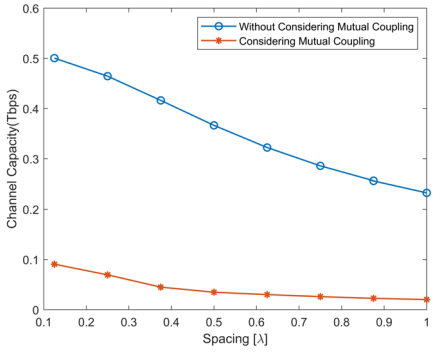

Fig. 5 UM-MIMO capacity with considering mutual coupling.

THz band and improve the communication capacity and distance.

4.2 The Impact of Mutual Coupling

Due to the AoSA structure, the effect of mutual coupling will only have the impact within the subarray. Based on the simulation parameters in Table 1 and the number of subarray is set to 10, varying the element spacing from $\lambda/8$ to λ, and the channel capacity of the UM-MIMO communication system can be calculated by Eq. (9) as shown in Fig. 5. The two curves in Fig. 5 represent the cases where mutual coupling is considered and not considered separately. When the effect of mutual coupling is not considered, the capacity steadily decreases by 18.8% on average for every $\lambda/8$ increase in antenna spacing. While the capacity is much lower when the mutual coupling is taken into consideration and the trend is more moderate as the average decrease of 10.35% per $\lambda/8$ increases. The two curves also show that when the antenna spacing exceeds $\lambda/2$, the channel capacity remains essentially constant after considering the effect of mutual coupling. Further, by subtracting the two curves in Fig. 5, the magnitude of the reduction in channel capacity after considering the coupling effect of the different spacings can be obtained. The drop in distance $\lambda/8$ is 0.42 Tbps, while the drop in distance λ is 0.21 Tbps. This is due to the increased antenna spacing actually reducing the effect of the mutual coupling on the system.

The above results show that the consideration of the mutual coupling effect significantly reduces the channel capacity and decreases the effect of mutual coupling as the element spacing grows.

5. Conclusion

In this letter, a UM-MIMO channel model based on the AoSA structure while taking into account the effect of mutual coupling is established. The coupling coefficient matrix of the subarray is derived by building a Thevenin equivalent circuit for the antenna. The transmission matrix and channel capacity equation of the UM-MIMO system are given considering the effect of mutual coupling. The simulation results show that increasing the number of antenna can significantly enhance the channel capacity while considering the mutual coupling will dramatically reduces it. A higher antenna spacing reduces the reduction in channel capacity due to the mutual coupling, and the channel capacity remains almost constant when the antenna spacing is greater than $\lambda/2$. The numerical results can be used as the reference for the design of the UM-MIMO system in 6G.

References

[1] M. Fujishima and S. Amakawa, "Integrated-circuit approaches to THz communications: Challenges, advances, and future prospects," IEICE Trans. Fundamentals, vol.E100-A, no.2, pp.516–523, Feb. 2017.
[2] I.F. Akyildiz, C. Han, Z. Hu, S. Nie, and J.M. Jornet, "Terahertz band communication: An old problem revisited and research directions for the next decade," IEEE Trans. Commun., vol.70, no.6, pp.4250–4285, 2022.
[3] A. Faisal, H. Sarieddeen, H. Dahrouj, T.Y. Al-Naffouri, and M.-S. Alouini, "Ultramassive MIMO systems at terahertz bands: Prospects and challenges," IEEE Veh. Technol. Mag., vol.15, no.4, pp.33–42, 2020.
[4] I.F. Akyildiz and J.M. Jornet, "Realizing ultra-massive MIMO (1024×1024) communication in the (0.06–10) terahertz band," Nano Communication Networks, vol.8, pp.46–54, 2016.
[5] C. Han, Y. Wang, Y. Li, Y. Chen, N.A. Abbasi, T. Kurner, and A.F. Molisch, "Terahertz wireless channels: A holistic survey on measurement, modeling, and analysis," IEEE Commun. Surveys Tuts., vol.24, no.3, pp.1670–1707, 2022.
[6] F. Zeng, X. Qiu, J. Li, B. Long, W. Su, and X. Chen, "Novel auto-calibration method for 7-elements hexagonal array with mutual coupling," IEICE Trans. Fundamentals, vol.E106-A, no.5, pp.858–862, May 2023.
[7] H. Wei, D. Wang, and X. You, "Reciprocity of mutual coupling for TDD massive MIMO systems," 2015 International Conference on Wireless Communications & Signal Processing (WCSP), pp.1–5, 2015.
[8] L. Zakrajsek, E. Einarsson, N. Thawdar, M. Medley, and J.M. Jornet, "Design of graphene-based plasmonic nano-antenna arrays in the presence of mutual coupling," 2017 11th European Conference on Antennas and Propagation (EUCAP), pp.1381–1385, 2017.
[9] B. Zhang, J.M. Jornet, I.F. Akyildiz, and Z.P. Wu, "Mutual coupling reduction for ultra-dense multiband plasmonic nano-antenna arrays using graphene-based frequency selective surface," IEEE Access, vol.7, pp.33214–33225, 2019.
[10] V. Verri, A. Radwan, M. D'Amico, and G. Gentili, "On the effect of chemical potential on mutual coupling between graphene patch

antennas at THz band," 2015 1st URSI Atlantic Radio Science Conference (URSI ATRASC), pp.1–4, 2015.

[11] C. Han, A.O. Bicen, and I.F. Akyildiz, "Multi-ray channel modeling and wideband characterization for wireless communications in the terahertz band," IEEE Trans. Wireless Commun., vol.14, no.5, pp.2402–2412, 2014.

[12] C. Han, J.M. Jornet, and I.F. Akyildiz, "Ultra-massive MIMO channel modeling for graphene-enabled terahertz-band communications," 2018 IEEE 87th Vehicular Technology Conference (VTC Spring), pp.1–5, 2018.

[13] C. Han and I.F. Akyildiz, "Three-dimensional end-to-end modeling and analysis for graphene-enabled terahertz band communications," IEEE Trans. Veh. Technol., vol.66, no.7, pp.5626–5634, 2016.